BULLETIN OF THE POLISH ACADEMY OF SCIENCES
TECHNICAL SCIENCES, Vol. 69(6), 2021, Article number: e138999
DOI: 10.24425/bpasts.2021.138999

Quasi-analytical solutions for the whirling motion of multi-stepped rotors with arbitrarily distributed mass unbalance running in anisotropic linear bearings

Michael KLANNER*, Marcel S. PREM, and Katrin ELLERMANN

Graz University of Technology, Institute of Mechanics, Kopernikusgasse 24/IV, 8010 Graz, Austria

Abstract. Vibration in rotating machinery leads to a series of undesired effects, e.g. noise, reduced service life or even machine failure. Even though there are many sources of vibrations in a rotating machine, the most common one is mass unbalance. Therefore, a detailed knowledge of the system behavior due to mass unbalance is crucial in the design phase of a rotor-bearing system. The modelling of the rotor and mass unbalance as a lumped system is a widely used approach to calculate the whirling motion of a rotor-bearing system. A more accurate representation of the real system can be found by a continuous model, especially if the mass unbalance is not constant and arbitrarily oriented in space. Therefore, a quasi-analytical method called Numerical Assembly Technique is extended in this paper, which allows for an efficient and accurate simulation of the unbalance response of a rotor-bearing system. The rotor shaft is modelled by the Rayleigh beam theory including rotatory inertia and gyroscopic effects. Rigid discs can be mounted onto the rotor and the bearings are modeled by linear translational/rotational springs/dampers, including cross-coupling effects. The effect of a constant axial force or torque on the system response is also examined in the simulation.

Key words: Numerical Assembly Technique; rotor dynamics; whirling motion; unbalance response; quasi-analytical solution.

1. INTRODUCTION

In the design of a rotor-bearing system, the critical speeds of the system play a major role, since they have to lie outside the operating speed range [1]. Therefore, the calculation of the critical speeds is mandatory for a reliable and safe rotor-bearing design. Valuable additional information can be found by calculating the unbalance response of the system, e.g. the vibration amplitudes at a certain critical speed, the optimal locations for balancing planes and the effectiveness of damping treatments [1].

The two most common techniques for the analysis of rotor-bearing systems are the Finite Element Method (FEM) [2] and the Transfer Matrix Method (TMM) [3]. Especially in TMM, most works in the literature apply a lumped parameter model, which is not effective and accurate when the shaft unbalance is arbitrarily distributed [4]. Therefore, Lee *et al.* [4] extended the classical TMM approach to include distributed unbalance in the shaft by a Fourier series representation. To fit the synchronous elliptical orbits of the rotor system, sixteen state variables are applied. In [5], the Finite Element Method (FEM) and a polynomial distribution of the unbalance is used in the unbalance response computation.

A method similar to TMM called Numerical Assembly Technique (NAT) is proposed in [6], which is used to simulate the harmonic vibrations of one-dimensional structures. Wu *et al.* [7] applied NAT to calculate the whirling speed and mode shapes of rotor models neglecting shear deformation and inertia effects. An extension of NAT to include distributed loading is given in [8], where the distributed load is approximated by a Fourier extension method. This extension is used in [9], to compute the unbalance response of a rotating multiple-stepped Rayleigh beam with attached discs running in anisotropic bearings. The influence of a generally distributed unbalance on the rotor vibrations is examined and the computational advantages compared to FEM are shown.

In the following, an extension of the authors' previous paper [9] is proposed by including the effects of axial loading (constant force and torque) on the lateral rotor vibrations and considering a general bearing model with cross-coupling. Therefore, simplified models of journal bearings can be introduced.

2. PROBLEM DESCRIPTION

In this section, a general rotor vibration problem with a multiple-stepped shaft running in anisotropic bearings is outlined. The shaft is modelled by the Rayleigh beam theory including the effects of constant axial loading and the bearings are represented by linear springs and dampers. Although, the Timoshenko beam theory, which also includes shear deformation, is more accurate, especially for beams with low slenderness, it leads to cumbersome mathematical expressions and a higher computational load. Therefore, the Rayleigh beam theory is preferred in this paper.

*e-mail: michael.klanner@tugraz.at

Manuscript submitted 2021-03-22, revised 2021-07-24, initially accepted for publication 2021-08-06, published in December 2021.

2.1. General rotor problem with constant axial loading

In Fig. 1, a multiple-stepped shaft supported by anisotropic bearings is shown. Translational and rotational springs and dampers including cross-coupling terms between the x- and y-direction are used to model the bearing characteristics. For clarity, only the translation springs in x- and y-direction are symbolized in Fig. 1. The shaft is running at constant spin speed Ω about the z-axis and several circular discs with mass $m^{(i)}$, mass moment of inertia about the x- and y-axis $\Theta_t^{(i)}$, and mass moment of inertia about the z-axis $\Theta_p^{(i)}$ are attached to the rotor. A generally distributed unbalance with the eccentricity $\varepsilon(z)$ and the angular position $\beta(z)$ between the positions $z_\ell = Z_{Au}$ and $z_\ell = Z_{Bu}$ is present in the shaft. Furthermore, the discs might also have mass unbalance given by the eccentricity $\varepsilon^{(i)}$ and angular position $\beta^{(i)}$.

A constant axial force P and axial twisting moment T are applied to the rotor boundaries. It is assumed that the axial loads remain parallel to the z-axis after deformation and that the axial force P follows the deformed rotor (no additional bending moment). Several other possibilities concerning the orientation of the axial loads after deformation are discussed in the literature [10–12], e.g. tangential (follower) forces and twisting moments.

The shaft (total length L) is divided by (N) stations into $M = (N-1)$ segments having a length $L_\ell = (Z_{i+1} - Z_i)\,(i = \ell)$. The rotor boundaries are located at the first (1) and last station (N) ($z = 0$ and $z = L$) and additional stations (i) have to be introduced if a discontinuity arises within the rotor. A local coordinate system $(O_\ell, x_\ell, y_\ell, z_\ell)$ for each segment ℓ is defined, which is centered at the location of the intermediate station (i) $(z = Z_i)$. The rotor has homogeneous material parameters and constant circular cross-sections within each rotor segment ℓ.

2.2. Rayleigh beam theory including axial effects

Each rotor segment ℓ is modelled by the well known Rayleigh beam theory, which includes inertia effects while neglecting shear deformation. As pointed out in [9], assuming a time dependency of the displacements $u_{x\ell}(z,t)$ (x-direction) and $u_{y\ell}(z,t)$ (y-direction) in the form

$$u_{x\ell}(z,t) = \tilde{u}_{x\ell}^{+}(z)\,\mathrm{e}^{\mathrm{j}\Omega t} + \tilde{u}_{x\ell}^{-}(z)\,\mathrm{e}^{-\mathrm{j}\Omega t}, \tag{1}$$

$$u_{y\ell}(z,t) = \tilde{u}_{y\ell}^{+}(z)\,\mathrm{e}^{\mathrm{j}\Omega t} + \tilde{u}_{y\ell}^{-}(z)\,\mathrm{e}^{-\mathrm{j}\Omega t}, \tag{2}$$

leads to a complete decoupling of the governing equations in terms of $\tilde{u}_{\bullet\ell}^{+}(z)$ and $\tilde{u}_{\bullet\ell}^{-}(z)$. Since the solutions of $\tilde{u}_{\bullet\ell}^{+}(z)$ and $\tilde{u}_{\bullet\ell}^{-}(z)$ have to be complex conjugated to yield real solutions for $u_{\bullet\ell}(z,t)$, only one has to be investigated. The governing equations for the steady-state harmonic unbalance response of a rotating Rayleigh beam with constant axial loading are given by

$$\frac{\mathrm{d}^4\tilde{u}_{x\ell}^{+}(z)}{\mathrm{d}z^4} + \left(\bar{\Omega}_\ell^2 - \bar{P}_\ell\right)\frac{\mathrm{d}^2\tilde{u}_{x\ell}^{+}(z)}{\mathrm{d}z^2} - \frac{\bar{\Omega}_\ell^2}{r_{G\ell}^2}\,\tilde{u}_{x\ell}^{+}(z) + \bar{T}_\ell\frac{\mathrm{d}^3\tilde{u}_{y\ell}^{+}(z)}{\mathrm{d}z^3} - 2\mathrm{j}\bar{\Omega}_\ell^2\frac{\mathrm{d}^2\tilde{u}_{y\ell}^{+}(z)}{\mathrm{d}z^2} = \frac{\bar{\Omega}_\ell^2}{2\,r_{G\ell}^2}\,\tilde{\varepsilon}_{+}(z), \tag{3}$$

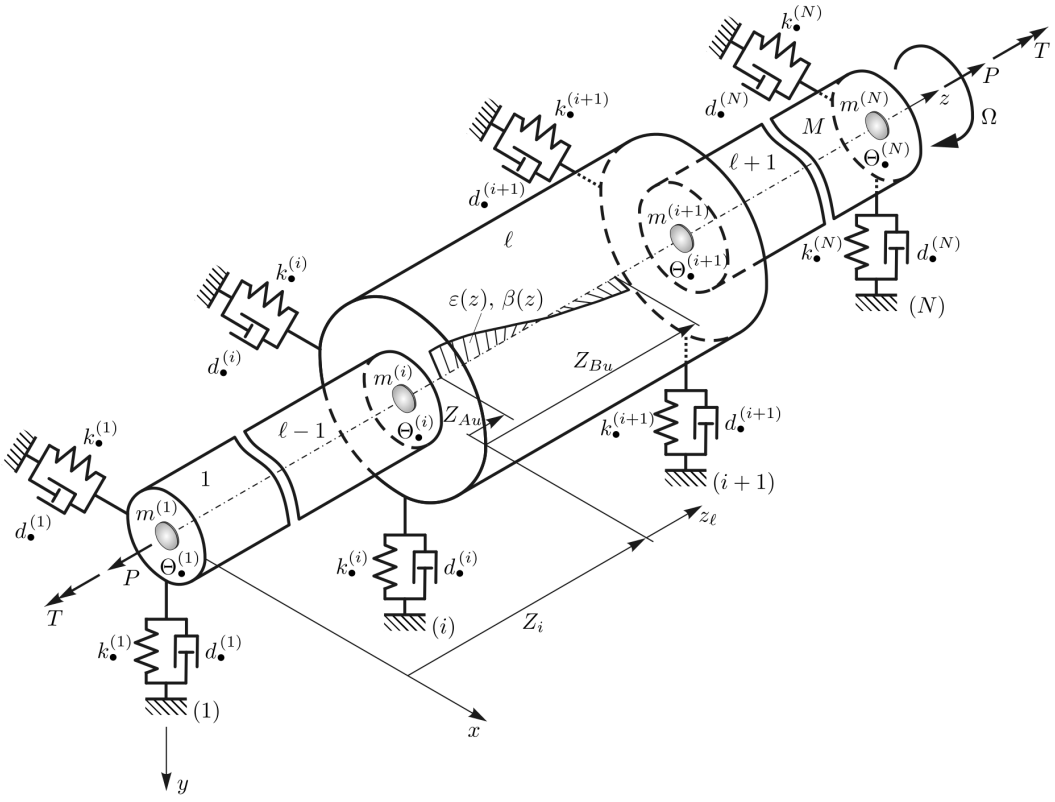

Fig. 1. General rotor problem with constant axial loading

$$\frac{\mathrm{d}^4\tilde{u}^+_{y\ell}(z)}{\mathrm{d}z^4}+\left(\bar{\Omega}^2_\ell-\bar{P}_\ell\right)\frac{\mathrm{d}^2\tilde{u}^+_{y\ell}(z)}{\mathrm{d}z^2}-\frac{\bar{\Omega}^2_\ell}{r^2_{G\ell}}\tilde{u}^+_{y\ell}(z) - \bar{T}_\ell\frac{\mathrm{d}^3\tilde{u}^+_{x\ell}(z)}{\mathrm{d}z^3}+2\,\mathrm{j}\,\bar{\Omega}^2_\ell\frac{\mathrm{d}^2\tilde{u}^+_{x\ell}(z)}{\mathrm{d}z^2}=-\frac{\mathrm{j}\,\bar{\Omega}^2_\ell}{2\,r^2_{G\ell}}\tilde{\varepsilon}_+(z), \quad (4)$$

with

$$\bar{\Omega}^2_\ell=\frac{\rho_\ell\,\Omega^2}{E_\ell},\quad r^2_{G\ell}=\frac{I_\ell}{A_\ell},\qquad \bar{T}_\ell=\frac{T}{E_\ell I_\ell},\qquad \bar{P}_\ell=\frac{P}{E_\ell I_\ell} \quad (5)$$

and E_ℓ Young's modulus, ρ_ℓ the material density, A_ℓ the cross-section area, Ω the rotor spin speed about the z-axis, P the constant normal force, T the constant axial torque, I_ℓ the planar second moments of area with respect to the x- and y-axis and $\tilde{\varepsilon}_+(z)=\varepsilon(z)\,\mathrm{e}^{\mathrm{j}\,\beta(z)}$ the complex unbalance. The governing equations of the rotating Rayleigh beam (equations (3) and (4)) are coupled through the gyroscopic effects and the constant axial torque and are consistent with the results shown in [4]. It is assumed that the displacements and eccentricities are small and therefore, only linear terms are considered in the unbalance force.

Apart from the displacements, additional field variables are required to fully describe the state of the rotor, which are given by

$$\begin{aligned}
\tilde{\varphi}^+_{x\ell}(z)&=-\frac{\mathrm{d}\tilde{u}^+_{y\ell}(z)}{\mathrm{d}z},\qquad \tilde{\varphi}^+_{y\ell}(z)=\frac{\mathrm{d}\tilde{u}^+_{x\ell}(z)}{\mathrm{d}z},\\
\tilde{M}^+_{x\ell}(z)&=-E_\ell I_\ell\frac{\mathrm{d}^2\tilde{u}^+_{y\ell}(z)}{\mathrm{d}z^2},\quad \tilde{M}^+_{y\ell}(z)=E_\ell I_\ell\frac{\mathrm{d}^2\tilde{u}^+_{x\ell}(z)}{\mathrm{d}z^2},\\
\tilde{Q}^+_{x\ell}(z)&=-E_\ell I_\ell\left(\frac{\mathrm{d}^3\tilde{u}^+_{x\ell}(z)}{\mathrm{d}z^3}+\bar{\Omega}^2_\ell\frac{\mathrm{d}\tilde{u}^+_{x\ell}(z)}{\mathrm{d}z}\right.\\
&\qquad\left.+\bar{T}_\ell\frac{\mathrm{d}^2\tilde{u}^+_{y\ell}(z)}{\mathrm{d}z^2}-2\,\mathrm{j}\,\bar{\Omega}^2_\ell\frac{\mathrm{d}\tilde{u}^+_{y\ell}(z)}{\mathrm{d}z}\right),\\
\tilde{Q}^+_{y\ell}(z)&=-E_\ell I_\ell\left(\frac{\mathrm{d}^3\tilde{u}^+_{y\ell}(z)}{\mathrm{d}z^3}+\bar{\Omega}^2_\ell\frac{\mathrm{d}\tilde{u}^+_{y\ell}(z)}{\mathrm{d}z}\right.\\
&\qquad\left.-\bar{T}_\ell\frac{\mathrm{d}^2\tilde{u}^+_{x\ell}(z)}{\mathrm{d}z^2}+2\,\mathrm{j}\,\bar{\Omega}^2_\ell\frac{\mathrm{d}\tilde{u}^+_{x\ell}(z)}{\mathrm{d}z}\right),
\end{aligned} \quad (6)$$

where $\tilde{\varphi}^+_{x\ell}(z)$ and $\tilde{\varphi}^+_{y\ell}(z)$ are the rotations about the x- and y-axis, $\tilde{M}^+_{x\ell}(z)$ and $\tilde{M}^+_{y\ell}(z)$ are the bending moments about the x- and y-axis and $\tilde{Q}^+_{x\ell}(z)$ and $\tilde{Q}^+_{y\ell}(z)$ are the shear forces in x- and y-direction.

The governing equations in equations (3) and (4) require certain boundary and interface conditions to yield a unique solution. Applying an equilibrium of forces and moments at the boundaries and taking into account that the constant axial loads remain parallel to the z-axis after deformation, lead to

$$\begin{aligned}
&a^{(1)}_{txx}\,\tilde{u}^+_{x1}(0)+\left(\mathrm{j}\,\Omega\,d^{(1)}_{txy}+k^{(1)}_{txy}\right)\tilde{u}^+_{y1}(0)\\
&\qquad-\tilde{Q}^+_{x1}(0)-P\,\tilde{\varphi}^+_{y1}(0)=\frac{m^{(1)}\,\tilde{\varepsilon}^{(1)}_+\,\Omega^2}{2},\\
&a^{(1)}_{tyy}\,\tilde{u}^+_{y1}(0)+\left(\mathrm{j}\,\Omega\,d^{(1)}_{tyx}+k^{(1)}_{tyx}\right)\tilde{u}^+_{x1}(0)\\
&\qquad-\tilde{Q}^+_{y1}(0)+P\,\tilde{\varphi}^+_{x1}(0)=-\frac{\mathrm{j}\,m^{(1)}\,\tilde{\varepsilon}^{(1)}_+\,\Omega^2}{2},\\
&a^{(1)}_{ryy}\,\tilde{\varphi}^+_{y1}(0)-\tilde{M}^+_{y1}(0)\\
&\qquad+\left(-\mathrm{j}\,\Omega^2\,\Theta^{(1)}_p+\mathrm{j}\,\Omega\,d^{(1)}_{ryx}+k^{(1)}_{ryx}+T\right)\tilde{\varphi}^+_{x1}(0)=0,\\
&a^{(1)}_{rxx}\,\tilde{\varphi}^+_{x1}(0)-\tilde{M}^+_{x1}(0)\\
&\qquad+\left(\mathrm{j}\,\Omega^2\,\Theta^{(1)}_p+\mathrm{j}\,\Omega\,d^{(1)}_{rxy}+k^{(1)}_{rxy}-T\right)\tilde{\varphi}^+_{y1}(0)=0,
\end{aligned} \quad (7)$$

for the left boundary and to

$$\begin{aligned}
&a^{(N)}_{txx}\,\tilde{u}^+_{xM}(L)+\left(\mathrm{j}\,\Omega\,d^{(N)}_{txy}+k^{(N)}_{txy}\right)\tilde{u}^+_{yM}(L)\\
&\qquad+\tilde{Q}^+_{xM}(L)+P\,\tilde{\varphi}^+_{yM}(L)=\frac{m^{(N)}\,\tilde{\varepsilon}^{(N)}_+\,\Omega^2}{2},\\
&a^{(N)}_{tyy}\,\tilde{u}^+_{yM}(L)+\left(\mathrm{j}\,\Omega\,d^{(N)}_{tyx}+k^{(N)}_{tyx}\right)\tilde{u}^+_{xM}(L)\\
&\qquad+\tilde{Q}^+_{yM}(L)-P\,\tilde{\varphi}^+_{xM}(L)=\frac{-\mathrm{j}\,m^{(N)}\,\tilde{\varepsilon}^{(N)}_+\,\Omega^2}{2},\\
&a^{(N)}_{ryy}\,\tilde{\varphi}^+_{yM}(L)+\tilde{M}^+_{yM}(L)\\
&\qquad+\left(-\mathrm{j}\,\Omega^2\,\Theta^{(N)}_p+\mathrm{j}\,\Omega\,d^{(N)}_{ryx}+k^{(N)}_{ryx}-T\right)\tilde{\varphi}^+_{xM}(L)=0,\\
&a^{(N)}_{rxx}\,\tilde{\varphi}^+_{xM}(L)+\tilde{M}^+_{xM}(L)\\
&\qquad+\left(\mathrm{j}\,\Omega^2\,\Theta^{(N)}_p+\mathrm{j}\,\Omega\,d^{(N)}_{rxy}+k^{(N)}_{rxy}+T\right)\tilde{\varphi}^+_{yM}(L)=0,
\end{aligned} \quad (8)$$

for the right boundary. Additionally, the continuity of the displacements and rotations results in

$$\begin{aligned}
&\tilde{u}^+_{x\ell}(Z_i^+)-\tilde{u}^+_{x\ell-1}(Z_i^-)=0,\quad \tilde{\varphi}^+_{y\ell}(Z_i^+)-\tilde{\varphi}^+_{y\ell-1}(Z_i^-)=0,\\
&a^{(i)}_{ryy}\,\tilde{\varphi}^+_{y\ell}(Z_i^+)-\tilde{M}^+_{y\ell}(Z_i^+)+\tilde{M}^+_{y\ell-1}(Z_i^-)\\
&\qquad+\left(-\mathrm{j}\,\Omega^2\,\Theta^{(i)}_p+\mathrm{j}\,\Omega\,d^{(i)}_{ryx}+k^{(i)}_{ryx}\right)\tilde{\varphi}^+_{x\ell}(Z_i^+)=0,\\
&a^{(i)}_{txx}\,\tilde{u}^+_{x\ell}(Z_i^+)+\left(\mathrm{j}\,\Omega\,d^{(i)}_{txy}+k^{(i)}_{txy}\right)\tilde{u}^+_{y\ell}(Z_i^+)\\
&\qquad-\tilde{Q}^+_{x\ell}(Z_i^+)+\tilde{Q}^+_{x\ell-1}(Z_i^-)=\frac{m^{(i)}\,\tilde{\varepsilon}^{(i)}_+\,\Omega^2}{2},\\
&\tilde{u}^+_{y\ell}(Z_i^+)-\tilde{u}^+_{y\ell-1}(Z_i^-)=0,\quad \tilde{\varphi}^+_{x\ell}(Z_i^+)-\tilde{\varphi}^+_{x\ell-1}(Z_i^-)=0,\\
&a^{(i)}_{rxx}\,\tilde{\varphi}^+_{x\ell}(Z_i^+)-\tilde{M}^+_{x\ell}(Z_i^+)+\tilde{M}^+_{x\ell-1}(Z_i^-)\\
&\qquad+\left(\mathrm{j}\,\Omega^2\,\Theta^{(i)}_p+\mathrm{j}\,\Omega\,d^{(i)}_{rxy}+k^{(i)}_{rxy}\right)\tilde{\varphi}^+_{y\ell}(Z_i^+)=0,\\
&a^{(i)}_{tyy}\,\tilde{u}^+_{y\ell}(Z_i^+)+\left(\mathrm{j}\,\Omega\,d^{(i)}_{tyx}+k^{(i)}_{tyx}\right)\tilde{u}^+_{x\ell}(Z_i^+)\\
&\qquad-\tilde{Q}^+_{y\ell}(Z_i^+)+\tilde{Q}^+_{y\ell-1}(Z_i^-)=-\frac{\mathrm{j}\,m^{(i)}\,\tilde{\varepsilon}^{(i)}_+\,\Omega^2}{2},
\end{aligned} \quad (9)$$

for an interface. In equations (7)–(9), the locations Z_i^- and Z_i^+ are infinitesimal to the left and right of the station (i), $k_\bullet^{(\star)}$ and $d_\bullet^{(\star)}$ are the spring and damping coefficients at station $\star$ and $a_{t\bullet}^{(\star)} = -\Omega^2 m^{(\star)} + \mathrm{j}\,\Omega\, d_{t\bullet}^{(\star)} + k_{t\bullet}^{(\star)}$ and $a_{r\bullet}^{(\star)} = -\Omega^2 \Theta_t^{(\star)} + \mathrm{j}\,\Omega\, d_{r\bullet}^{(\star)} + k_{r\bullet}^{(\star)}$. The governing equations of the rotating Rayleigh beam given in equations (3) and (4), the boundary conditions in equations (7) and (8) and the interface conditions in equation (9) form a well-posed problem, which can be uniquely solved by analytical or numerical methods.

3. NUMERICAL ASSEMBLY TECHNIQUE

The Numerical Assembly Technique (NAT) is a semi-analytical method, which applies the analytical solutions of the governing equations to fit the boundary and interface conditions. This leads to a system of linear equations, which can be solved for the unknown contribution factors. The general analytical solution of the governing equations $\tilde{u}_{\bullet\ell}^+(z_\ell)$ is given by the superposition of the homogeneous solution $\tilde{u}_{h\bullet\ell}^+(z_\ell)$ ($\tilde{\varepsilon}_+(z) = 0$) and the particular solution $\tilde{u}_{p\bullet\ell}^+(z_\ell)$, which are derived in the following sections.

3.1. Analytical solution of the homogeneous equation

Setting the complex unbalance $\tilde{\varepsilon}_+(z) = 0$ and plugging the assumed solutions

$$\tilde{u}_{hx\ell}^+(z_\ell) = c_{u_x\ell}\, \mathrm{e}^{\mathrm{j}kz_\ell}, \tag{10}$$

$$\tilde{u}_{hy\ell}^+(z_\ell) = c_{u_y\ell}\, \mathrm{e}^{\mathrm{j}kz_\ell}, \tag{11}$$

into equations (3) and (4) leads to the system of linear equations

$$\boldsymbol{A} \begin{bmatrix} c_{u_x\ell} \\ c_{u_y\ell} \end{bmatrix} = \begin{bmatrix} 0 \\ 0 \end{bmatrix}, \tag{12}$$

with

$$\boldsymbol{A} = \begin{bmatrix} k^4 - \left(\bar{\Omega}_\ell^2 - \bar{P}_\ell\right) k^2 - \dfrac{\bar{\Omega}_\ell^2}{r_{G\ell}^2} & -\mathrm{j}\,\bar{T}_\ell k^3 + 2\mathrm{j}\,\bar{\Omega}_\ell^2 k^2 \\ \mathrm{j}\,\bar{T}_\ell k^3 - 2\mathrm{j}\,\bar{\Omega}_\ell^2 k^2 & k^4 - \left(\bar{\Omega}_\ell^2 - \bar{P}_\ell\right) k^2 - \dfrac{\bar{\Omega}_\ell^2}{r_{G\ell}^2} \end{bmatrix} \tag{13}$$

which only has a non-trivial solution if

$$\left(k^4 - \left(\bar{\Omega}_\ell^2 - \bar{P}_\ell\right) k^2 - \frac{\bar{\Omega}_\ell^2}{r_{G\ell}^2}\right)^2 - \left(-\bar{T}_\ell k^3 + 2\,\bar{\Omega}_\ell^2 k^2\right)^2 = 0. \tag{14}$$

Equation (14) can be split into two separate characteristic equations

$$\begin{aligned} k^4 - \bar{T}_\ell k^3 + \left(\bar{P}_\ell + \bar{\Omega}_\ell^2\right) k^2 - \frac{\bar{\Omega}_\ell^2}{r_{G\ell}^2} &= 0, \\ k^4 + \bar{T}_\ell k^3 + \left(\bar{P}_\ell - 3\,\bar{\Omega}_\ell^2\right) k^2 - \frac{\bar{\Omega}_\ell^2}{r_{G\ell}^2} &= 0, \end{aligned} \tag{15}$$

which have the solutions $k_{1\ell}$–$k_{4\ell}$ (first characteristic equation) and $k_{5\ell}$–$k_{8\ell}$ (second characteristic equation). Even though, analytical expressions of the roots of the characteristic polynomial exist, they are impractical in a numerical implementation and additionally might become unstable due to rounding errors. Therefore, stable numerical algorithms are preferred for their computation.

The constants $c_{u_x\ell}$ and $c_{u_y\ell}$ are not independent. For the first four solutions ($k_{1\ell}$–$k_{4\ell}$), the relation is $c_{u_y\ell} = -\mathrm{j}\,c_{u_x\ell}$ and for the last four solutions ($k_{5\ell}$–$k_{8\ell}$) the relation is $c_{u_y\ell} = \mathrm{j}\,c_{u_x\ell}$. The general homogeneous solution is therefore given by

$$\tilde{u}_{hx\ell}^+(z_\ell) = \sum_{i=1}^{8} c_{i\ell}\, \mathrm{e}^{\mathrm{j}\,k_{i\ell}\left(z_\ell - \mathrm{H}\left(-\mathrm{Im}\{k_{i\ell}\}\right) L_\ell\right)}, \tag{16}$$

$$\begin{aligned} \tilde{u}_{hy\ell}^+(z_\ell) = -\mathrm{j} \Bigg(& \sum_{i=1}^{4} c_{i\ell}\, \mathrm{e}^{\mathrm{j}\,k_{i\ell}\left(z_\ell - \mathrm{H}\left(-\mathrm{Im}\{k_{i\ell}\}\right) L_\ell\right)} \\ & - \sum_{i=5}^{8} c_{i\ell}\, \mathrm{e}^{\mathrm{j}\,k_{i\ell}\left(z_\ell - \mathrm{H}\left(-\mathrm{Im}\{k_{i\ell}\}\right) L_\ell\right)} \Bigg) \end{aligned} \tag{17}$$

with $c_{1\ell}$–$c_{8\ell}$ arbitrary constants, $\mathrm{Im}\{\bullet\}$ the imaginary part and the Heaviside step function

$$\mathrm{H}(x) = \begin{cases} 0, & x \le 0 \\ 1, & x > 0 \end{cases}. \tag{18}$$

The lower index $\bullet_h$ indicates the homogeneous solution of the differential equations. In equations (16) and (17) a scaling of the parts with growing exponentials has been applied, which guaranties that the amplitude of each function term remains smaller or equal to 1 within the segment span ($0 \le z_\ell \le L_\ell$). This has certain advantages in the numerical implementation.

A complete description of the state within the rotor segment ℓ is given, if not only the displacements, but also the rotations, bending moments and shear forces are known. If the state variables and arbitrary constants are gathered in the column vectors

$$\begin{aligned} \tilde{\mathbf{x}}_{h\ell}^+(z_\ell) = \Big[& \tilde{u}_{hx\ell}^+(z_\ell),\ \tilde{u}_{hy\ell}^+(z_\ell),\ \tilde{\varphi}_{hy\ell}^+(z_\ell),\ \tilde{\varphi}_{hx\ell}^+(z_\ell), \\ & \tilde{M}_{hy\ell}^+(z_\ell),\ \tilde{M}_{hx\ell}^+(z_\ell),\ \tilde{Q}_{hx\ell}^+(z_\ell),\ \tilde{Q}_{hy\ell}^+(z_\ell) \Big]^{\mathrm{T}} \end{aligned}$$

and

$$\mathbf{c}_\ell = [c_{1\ell},\ c_{2\ell},\ c_{3\ell},\ c_{4\ell}, c_{5\ell},\ c_{6\ell},\ c_{7\ell},\ c_{8\ell}]^{\mathrm{T}},$$

the state within a rotor segment ℓ can be defined by a compact matrix equation as

$$\tilde{\mathbf{x}}_{h\ell}^+(z_\ell) = \mathbf{B}_\ell(z_\ell)\, \mathbf{c}_\ell, \tag{19}$$

where the upper index $\bullet^{\mathrm{T}}$ denotes the transpose of a vector or matrix. The state variable matrix is given by

$$\mathbf{B}_\ell = \begin{bmatrix} E_1 & E_2 & E_3 & E_4 \\ -\mathrm{j}E_1 & -\mathrm{j}E_2 & -\mathrm{j}E_3 & -\mathrm{j}E_4 \\ k_{\varphi 1}E_1 & k_{\varphi 2}E_2 & k_{\varphi 3}E_3 & k_{\varphi 4}E_4 \\ \mathrm{j}k_{\varphi 1}E_1 & \mathrm{j}k_{\varphi 2}E_2 & \mathrm{j}k_{\varphi 3}E_3 & \mathrm{j}k_{\varphi 4}E_4 \\ -k_{M1}E_1 & -k_{M2}E_2 & -k_{M3}E_3 & -k_{M4}E_4 \\ -\mathrm{j}k_{M1}E_1 & -\mathrm{j}k_{M2}E_2 & -\mathrm{j}k_{M3}E_3 & -\mathrm{j}k_{M4}E_4 \\ k_{Q1}E_1 & k_{Q2}E_2 & k_{Q3}E_3 & k_{Q4}E_4 \\ -\mathrm{j}k_{Q1}E_1 & -\mathrm{j}k_{Q2}E_2 & -\mathrm{j}k_{Q3}E_3 & -\mathrm{j}k_{Q4}E_4 \end{bmatrix} \begin{bmatrix} E_5 & E_6 & E_7 & E_8 \\ \mathrm{j}E_5 & \mathrm{j}E_6 & \mathrm{j}E_7 & \mathrm{j}E_8 \\ k_{\varphi 5}E_5 & k_{\varphi 6}E_6 & k_{\varphi 7}E_7 & k_{\varphi 8}E_8 \\ -\mathrm{j}k_{\varphi 5}E_5 & -\mathrm{j}k_{\varphi 6}E_6 & -\mathrm{j}k_{\varphi 7}E_7 & -\mathrm{j}k_{\varphi 8}E_8 \\ -k_{M5}E_5 & -k_{M6}E_6 & -k_{M7}E_7 & -k_{M8}E_8 \\ \mathrm{j}k_{M5}E_5 & \mathrm{j}k_{M6}E_6 & \mathrm{j}k_{M7}E_7 & \mathrm{j}k_{M8}E_8 \\ k_{Q5}E_5 & k_{Q6}E_6 & k_{Q7}E_7 & k_{Q8}E_8 \\ \mathrm{j}k_{Q5}E_5 & \mathrm{j}k_{Q6}E_6 & \mathrm{j}k_{Q7}E_7 & \mathrm{j}k_{Q8}E_8 \end{bmatrix} \tag{20}$$

with $k_{\varphi\bullet} = \mathrm{j}k_{\bullet\ell}$, $k_{M\bullet} = E_\ell I_\ell k_{\bullet\ell}^2$, $k_{Qi} = \mathrm{j}E_\ell I_\ell k_{i\ell}\left(k_{i\ell}^2 - \bar{T}_\ell k_{i\ell} + \bar{\Omega}_\ell^2\right)$ $(i = 1,\ldots,4)$, $k_{Qi} = \mathrm{j}E_\ell I_\ell k_{i\ell}\left(k_{i\ell}^2 + \bar{T}_\ell k_{i\ell} - 3\bar{\Omega}_\ell^2\right)$ $(i = 5,\ldots,8)$ and $E_\bullet = \mathrm{e}^{\mathrm{j}k_{\bullet\ell}(z_\ell - \mathrm{H}(-\mathrm{Im}\{k_{\bullet\ell}\})L_\ell)}$. The relations in equation (6) have been used to derive equations (19) and (20).

3.2. Particular solutions for an arbitrarily distributed unbalance

The particular solutions $\tilde{u}_{px\ell}^+(z_\ell)$ and $\tilde{u}_{py\ell}^+(z_\ell)$ fulfil the right hand side of the harmonic governing equations (equations (3) and (4)). The Fourier transform [13], the residue theorem and Jordan's lemma [14] and the Green's function method [15] are used to derive the particular solutions for an arbitrarily distributed mass unbalance.

First, the solutions for a concentrated unbalance located at a certain position $z_\ell = Z_\varepsilon$, which is given by

$$\tilde{\varepsilon}_+(z) = \tilde{\varepsilon}_{P+}\,\delta(z_\ell - Z_\varepsilon) \tag{21}$$

with $\delta(\bullet)$ the Dirac delta function and $\tilde{\varepsilon}_{P+}$ the complex amplitude of the unbalance (eccentricity times a fictitious length), is computed. If a concentrated unbalance is added in this form, no additional mass is included at the position Z_ε. The magnitude of the unbalance force is defined by the density ρ_ℓ and area A_ℓ of the rotor segment ℓ, the complex amplitude $\tilde{\varepsilon}_{P+}$ and the square of the spin speed Ω. Applying the Fourier transform [13] with respect to the spatial coordinate z_ℓ to equations (3) and (4), leads to the system of linear equations

$$\boldsymbol{A}\begin{bmatrix} \hat{u}_{px\ell}^+(k) \\ \hat{u}_{py\ell}^+(k) \end{bmatrix} = \begin{bmatrix} \frac{\bar{\Omega}_\ell^2}{2r_{G\ell}^2}\hat{\varepsilon}_+(k) \\ -\frac{\mathrm{j}\bar{\Omega}_\ell^2}{2r_{G\ell}^2}\hat{\varepsilon}_+(k) \end{bmatrix}, \tag{22}$$

with $\hat{\bullet}(k)$ the Fourier transform of $\bullet(z_\ell)$. Using the Fourier transform of the concentrated unbalance

$$\hat{\varepsilon}_+(k) = \tilde{\varepsilon}_{P+}\,\mathrm{e}^{-\mathrm{j}kZ_\varepsilon} \tag{23}$$

and solving the system of linear equations for the unknown displacements lead to

$$\begin{aligned} \hat{u}_{px\ell}^+(k) &= \frac{\bar{\Omega}_\ell^2}{2r_{G\ell}^2}\frac{\tilde{\varepsilon}_{P+}\,\mathrm{e}^{-\mathrm{j}kZ_\varepsilon}}{k^4 - \bar{T}_\ell k^3 + \left(\bar{P}_\ell + \bar{\Omega}_\ell^2\right)k^2 - \frac{\bar{\Omega}_\ell^2}{r_{G\ell}^2}} \\ &= \frac{\bar{\Omega}_\ell^2}{2r_{G\ell}^2}\frac{\tilde{\varepsilon}_{P+}\,\mathrm{e}^{-\mathrm{j}kZ_\varepsilon}}{(k-k_{1\ell})(k-k_{2\ell})(k-k_{3\ell})(k-k_{4\ell})}, \end{aligned} \tag{24}$$

and $\hat{u}_{py\ell}^+(k) = -\mathrm{j}\hat{u}_{px\ell}^+(k)$. The inverse Fourier transform [13] results in the integral

$$\tilde{u}_{px\ell}^+(z_\ell) = \int_{-\infty}^{\infty} \frac{\bar{\Omega}_\ell^2\,\tilde{\varepsilon}_{P+}\,\mathrm{e}^{\mathrm{j}k(z_\ell - Z_\varepsilon)}\,\mathrm{d}k}{4\pi r_{G\ell}^2(k-k_{1\ell})(k-k_{2\ell})(k-k_{3\ell})(k-k_{4\ell})}, \tag{25}$$

which can be evaluated with the residue theorem [14]. In all practical cases, two of the four roots $k_{1\ell}$–$k_{4\ell}$ are non-real and complex conjugated and two are distinct real. The final results for the displacement in x-direction due to a concentrated unbalance are given by

$$\begin{aligned} \tilde{u}_{px\ell}^+(z_\ell, Z_\varepsilon) = \Bigg(&\frac{2\,\mathrm{e}^{\mathrm{j}\alpha_{1\ell}(z_\ell - Z_\varepsilon)}}{(\alpha_{1\ell}-\alpha_{2\ell})(\alpha_{1\ell}-\alpha_{3\ell})(\alpha_{1\ell}-\alpha_{4\ell})} \\ &+ \frac{\mathrm{e}^{\mathrm{j}\alpha_{3\ell}(z_\ell - Z_\varepsilon)}}{(\alpha_{3\ell}-\alpha_{1\ell})(\alpha_{3\ell}-\alpha_{2\ell})(\alpha_{3\ell}-\alpha_{4\ell})} \quad \text{for} \quad z_\ell > Z_\varepsilon \\ &+ \frac{\mathrm{e}^{\mathrm{j}\alpha_{4\ell}(z_\ell - Z_\varepsilon)}}{(\alpha_{4\ell}-\alpha_{1\ell})(\alpha_{4\ell}-\alpha_{2\ell})(\alpha_{4\ell}-\alpha_{3\ell})}\Bigg)\frac{\mathrm{j}\bar{\Omega}_\ell^2\,\tilde{\varepsilon}_{P+}}{4r_{G\ell}^2}, \end{aligned} \tag{26}$$

$$\begin{aligned} \tilde{u}_{px\ell}^+(z_\ell, Z_\varepsilon) = \Bigg(&\frac{-2\,\mathrm{e}^{\mathrm{j}\alpha_{2\ell}(z_\ell - Z_\varepsilon)}}{(\alpha_{2\ell}-\alpha_{1\ell})(\alpha_{2\ell}-\alpha_{3\ell})(\alpha_{2\ell}-\alpha_{4\ell})} \\ &- \frac{\mathrm{e}^{\mathrm{j}\alpha_{3\ell}(z_\ell - Z_\varepsilon)}}{(\alpha_{3\ell}-\alpha_{1\ell})(\alpha_{3\ell}-\alpha_{2\ell})(\alpha_{3\ell}-\alpha_{4\ell})} \quad \text{for} \quad z_\ell < Z_\varepsilon \\ &- \frac{\mathrm{e}^{\mathrm{j}\alpha_{4\ell}(z_\ell - Z_\varepsilon)}}{(\alpha_{4\ell}-\alpha_{1\ell})(\alpha_{4\ell}-\alpha_{2\ell})(\alpha_{4\ell}-\alpha_{3\ell})}\Bigg)\frac{\mathrm{j}\bar{\Omega}_\ell^2\,\tilde{\varepsilon}_{P+}}{4r_{G\ell}^2}, \end{aligned} \tag{27}$$

where $\alpha_{1\ell}$ is the complex root with positive imaginary part $(\mathrm{Im}\{k_{\bullet\ell}\} > 0)$, $\alpha_{2\ell}$ is the complex root with negative imaginary part $(\mathrm{Im}\{k_{\bullet\ell}\} < 0)$ and $\alpha_{3\ell}$ and $\alpha_{4\ell}$ are the distinct real roots $(\mathrm{Im}\{k_{\bullet\ell}\} = 0)$. The displacement in y-direction is simply found by $\tilde{u}_{py\ell}^+(z_\ell, Z_\varepsilon) = -\mathrm{j}\tilde{u}_{px\ell}^+(z_\ell, Z_\varepsilon)$.

The rotations, bending moments and the shear forces can be computed by equation (6) and all field variables can be gathered in the column vector $\tilde{\mathbf{x}}_{p\ell}^+(z_\ell, Z_\varepsilon)$ with the ordering equivalent to the homogeneous solutions $\tilde{\mathbf{x}}_{h\ell}^+(z_\ell)$. The particular solution functions for distributed unbalances are derived using the Green's function method, which uses the response due to a unit concentrated unbalance (Green's function) and an integration

over the distributed unbalance region [15]. Multiplying equations (26) and (27) with $\tilde{\varepsilon}_+(z_u) = \varepsilon(z_u)\,\mathrm{e}^{\mathrm{j}\,\beta(z_u)}$, setting $\tilde{\varepsilon}_{P+} = 1$ and integrating over the unbalance region from $z_u = Z_{Au}$ to $z_u = Z_{Bu}$ lead to the general particular solutions for distributed unbalances in integral form

$$\tilde{u}^+_{px\ell}(\bar{z}_\ell) = \frac{Z_{Bu} - Z_{Au}}{2} \int_{-1}^{1} \tilde{\varepsilon}_+(\bar{z}_u)\, \tilde{u}^+_{px\ell}(\bar{z}_\ell, \bar{z}_u)\, \mathrm{d}\bar{z}_u, \tag{28}$$

where the change of variables

$$\bar{z}_u = \frac{2\,z_u - Z_{Bu} - Z_{Au}}{Z_{Bu} - Z_{Au}}, \qquad \bar{z}_\ell = \frac{2\,z_\ell - Z_{Bu} - Z_{Au}}{Z_{Bu} - Z_{Au}} \tag{29}$$

has been applied. The Fourier extension (continuation) method [16, 17] is used to approximate the generally distributed unbalance, which leads to

$$\tilde{\varepsilon}_+(\bar{z}_u) \approx \frac{1}{\sqrt{2\,T}} \sum_{k=-n}^{n} d_{uk}\, \mathrm{e}^{\mathrm{j}\frac{k\pi}{T}\bar{z}_u} \quad \text{with} \quad -1 \le \bar{z}_u \le 1 \tag{30}$$

with $T > 1$ and n corresponding to the order of the approximation. The numerical discrete Fourier extension with equispaced sampling points, presented in [16], allows an efficient computation of the factors d_{uk}. Plugging equations (26) and (27) and equation (30) into equation (28) results in

$$\begin{aligned}
\tilde{u}^+_{px\ell}(\bar{z}_\ell) = {} & \frac{\mathrm{j}\,\bar{\Omega}^2_\ell\,(Z_{Bu} - Z_{Au})^4}{\sqrt{2\,T}\,64\,r^2_{G\ell}} \sum_{k=-n}^{n} \int_{-1}^{1} d_{uk}\, \mathrm{e}^{\mathrm{j}\frac{k\pi}{T}\bar{z}_u} \\
& \begin{cases}
\dfrac{2\,\mathrm{e}^{\mathrm{j}\,\bar{\alpha}_{1\ell}(\bar{z}_\ell - \bar{z}_u)}}{(\bar{\alpha}_{1\ell} - \bar{\alpha}_{2\ell})(\bar{\alpha}_{1\ell} - \bar{\alpha}_{3\ell})(\bar{\alpha}_{1\ell} - \bar{\alpha}_{4\ell})} \\
\quad + \dfrac{\mathrm{e}^{\mathrm{j}\,\bar{\alpha}_{3\ell}(\bar{z}_\ell - \bar{z}_u)}}{(\bar{\alpha}_{3\ell} - \bar{\alpha}_{1\ell})(\bar{\alpha}_{3\ell} - \bar{\alpha}_{2\ell})(\bar{\alpha}_{3\ell} - \bar{\alpha}_{4\ell})} & \bar{z}_\ell \ge \bar{z}_u \\
\quad + \dfrac{\mathrm{e}^{\mathrm{j}\,\bar{\alpha}_{4\ell}(\bar{z}_\ell - \bar{z}_u)}}{(\bar{\alpha}_{4\ell} - \bar{\alpha}_{1\ell})(\bar{\alpha}_{4\ell} - \bar{\alpha}_{2\ell})(\bar{\alpha}_{4\ell} - \bar{\alpha}_{3\ell})}, & \\
\qquad\qquad\qquad\qquad\qquad\qquad\qquad\qquad\qquad\qquad \mathrm{d}\bar{z}_u, & \\
-\dfrac{2\,\mathrm{e}^{\mathrm{j}\,\bar{\alpha}_{2\ell}(\bar{z}_\ell - \bar{z}_u)}}{(\bar{\alpha}_{2\ell} - \bar{\alpha}_{1\ell})(\bar{\alpha}_{2\ell} - \bar{\alpha}_{3\ell})(\bar{\alpha}_{2\ell} - \bar{\alpha}_{4\ell})} \\
\quad - \dfrac{\mathrm{e}^{\mathrm{j}\,\bar{\alpha}_{3\ell}(\bar{z}_\ell - \bar{z}_u)}}{(\bar{\alpha}_{3\ell} - \bar{\alpha}_{1\ell})(\bar{\alpha}_{3\ell} - \bar{\alpha}_{2\ell})(\bar{\alpha}_{3\ell} - \bar{\alpha}_{4\ell})} & \bar{z}_\ell \le \bar{z}_u \\
\quad - \dfrac{\mathrm{e}^{\mathrm{j}\,\bar{\alpha}_{4\ell}(\bar{z}_\ell - \bar{z}_u)}}{(\bar{\alpha}_{4\ell} - \bar{\alpha}_{1\ell})(\bar{\alpha}_{4\ell} - \bar{\alpha}_{2\ell})(\bar{\alpha}_{4\ell} - \bar{\alpha}_{3\ell})}, &
\end{cases}
\end{aligned} \tag{31}$$

where $\bar{\alpha}_{\bullet\ell} = \alpha_{\bullet\ell}\,\dfrac{Z_{Bu} - Z_{Au}}{2}$ are the normalized wave numbers. The integrals in equation (31) can be analytically evaluated in closed-form, which requires a distinction of three cases depending on the coordinate $\bar{z}_\ell$. Similar to the concentrated unbalance, the displacement in y-direction can be calculated by $\tilde{u}^+_{py\ell}(\bar{z}_\ell) = -\mathrm{j}\,\tilde{u}^+_{px\ell}(\bar{z}_\ell)$ and all other field variables are given through equation (6).

3.3. Fitting the boundary and interface conditions

Plugging the total solution $\tilde{\mathbf{x}}^+_\ell(z_\ell) = \tilde{\mathbf{x}}^+_{h\ell}(z_\ell) + \tilde{\mathbf{x}}^+_{p\ell}(z_\ell)$ of each rotor segment ℓ into the boundary and interface conditions (equations (7)–(9)) leads to a system of linear equations $\mathbf{A}\,\mathbf{c} = \mathbf{b}$ with $\mathbf{c} = [\mathbf{c}_1, \cdots, \mathbf{c}_\ell, \cdots, \mathbf{c}_M]^{\mathrm{T}}$ the arbitrary constants of the homogenous solutions. The system matrix $\mathbf{A}$ (size $8M \times 8M$) depends only on the concentrated elements at the stations, while the right-hand side vector $\mathbf{b}$ (size $8M \times 1$) is additionally affected by the rotor unbalance. The unknown constants $\mathbf{c}$ are the solution of the system of linear equations $\mathbf{A}\,\mathbf{c} = \mathbf{b}$, which uniquely define the state variables for the whole rotor. The system matrix $\mathbf{A}$ has a banded structure since it is an assembly of the local system matrices A_ℓ of each rotor segment ℓ.

4. NUMERICAL EXAMPLES

In this section, NAT is used to calculate the steady-state harmonic response of two different rotor-bearing systems. The first system is rather simple to illustrate the effects of the axial loadings and the distributed unbalance, while the second system is more realistic and is used to show the efficiency and accuracy of NAT.

The first example is a four-stepped rotor, which is shown in Fig. 2. Three rigid discs are mounted to the rotor, which is supported by isotropic and symmetrical bearings. The disc at station (3) has a mass unbalance $\varepsilon^{(3)} = 0.03$ mm at the angular position $\beta^{(3)} = 30^\circ$ and a distribute unbalance $\varepsilon(z) = -0.2 + 0.02\cos(-1.05 + 8\,z)\,\mathrm{e}^{0.5\,z}$ (mm) with the angular position $\beta(z) = -15 + 385\,z\,(^\circ)$ is present in the rotor segments 4 and 5.

The rotor is made of aluminium ($E = 7 \cdot 10^{10}$ N/m^2, $\rho = 2700$ kg/m^3) and the circular cross-sections in segment 1, 2 and 5 have a radius of 0.020 m, in segment 3 of 0.025 m and in segment 4 of 0.030 m, leading to a total mass of 4.76 kg. The total length of the rotor is 1.04 m, which leads to a ratio of the rotor length to the maximum diameter of 17.33 allowing the use of the Rayleigh beam theory. The parameters of the concentrated elements at the stations are listed in Table 1, where the coefficients of the isotropic and symmetrical bearings are taken from [18].

The proposed NAT is implemented in *MATLAB*® *R2020a*. To verify the calculated results and to assess the computational efficiency of NAT, the FEM Matlab code presented by Friswell

Table 1
Parameters of the bearings and discs for the first example

(i)	Z_i (m)	m (kg)	Θ_t (kgm^2)	Θ_p (kgm^2)	k_x (N/m)	k_y (N/m)	$k_{xy} = k_{yx}$ (N/m)	$d_x = d_y$ (Ns/m)
1	0.00	0	0	0	0	0	0	0
2	0.15	0	0	0	1e7	1e7	5e6	2000
3	0.31	15	0.01	0.015	0	0	0	0
4	0.51	25	0.015	0.025	0	0	0	0
5	0.71	20	0.015	0.012	0	0	0	0
6	1.04	0	0	0	1e7	1e7	5e6	2000

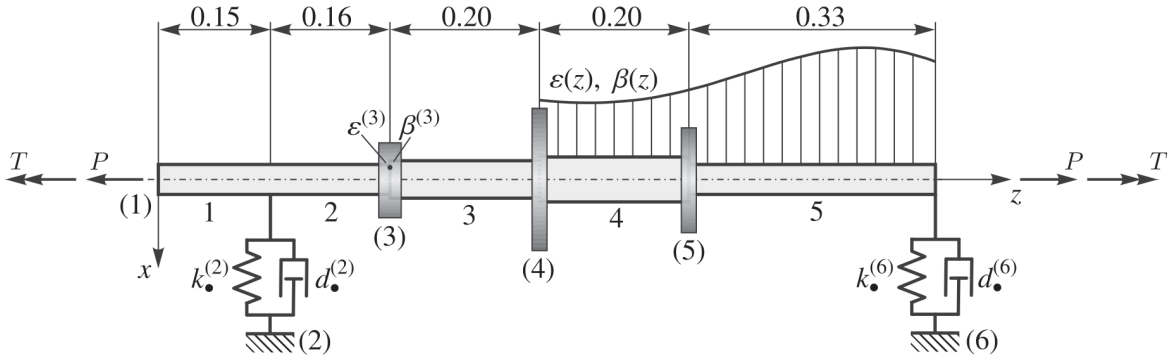

Fig. 2. Configuration of the first example rotor with distributed unbalance and axial loading

et al. [19] is used for comparison. A FEM element size of 0.01 m is applied to guarantee accurate reference results.

In Fig. 3, the unbalance response of the rotor-bearing system for different spin speeds and axial loads is shown. The parameter a represents the major axis of the elliptical whirling orbit at the arbitrary rotor location $z = 0.46$ m. The high values of the axial loadings P and T, used in Fig. 3, may result in a buckling or fatigue of real shafts (see e.g. [20]) and are only applied to clearly illustrate their effects on the unbalance response. Especially, the values of the constant axial torque would lead to very high tangential stresses and cracking of the shaft. Realistic values of the torque have only a minor impact on the unbalance response. It is apparent from Figs. 3a and 3b that a compression force leads to a decrease of the critical speeds of the rotor. This is consistent with the results given in the literature, e.g. [20]. Similarly, a constant axial torque also leads to a decrease of the critical speeds, which is clearly shown in Figs. 3c and 3d. This effect has also been verified by e.g. Eshleman and

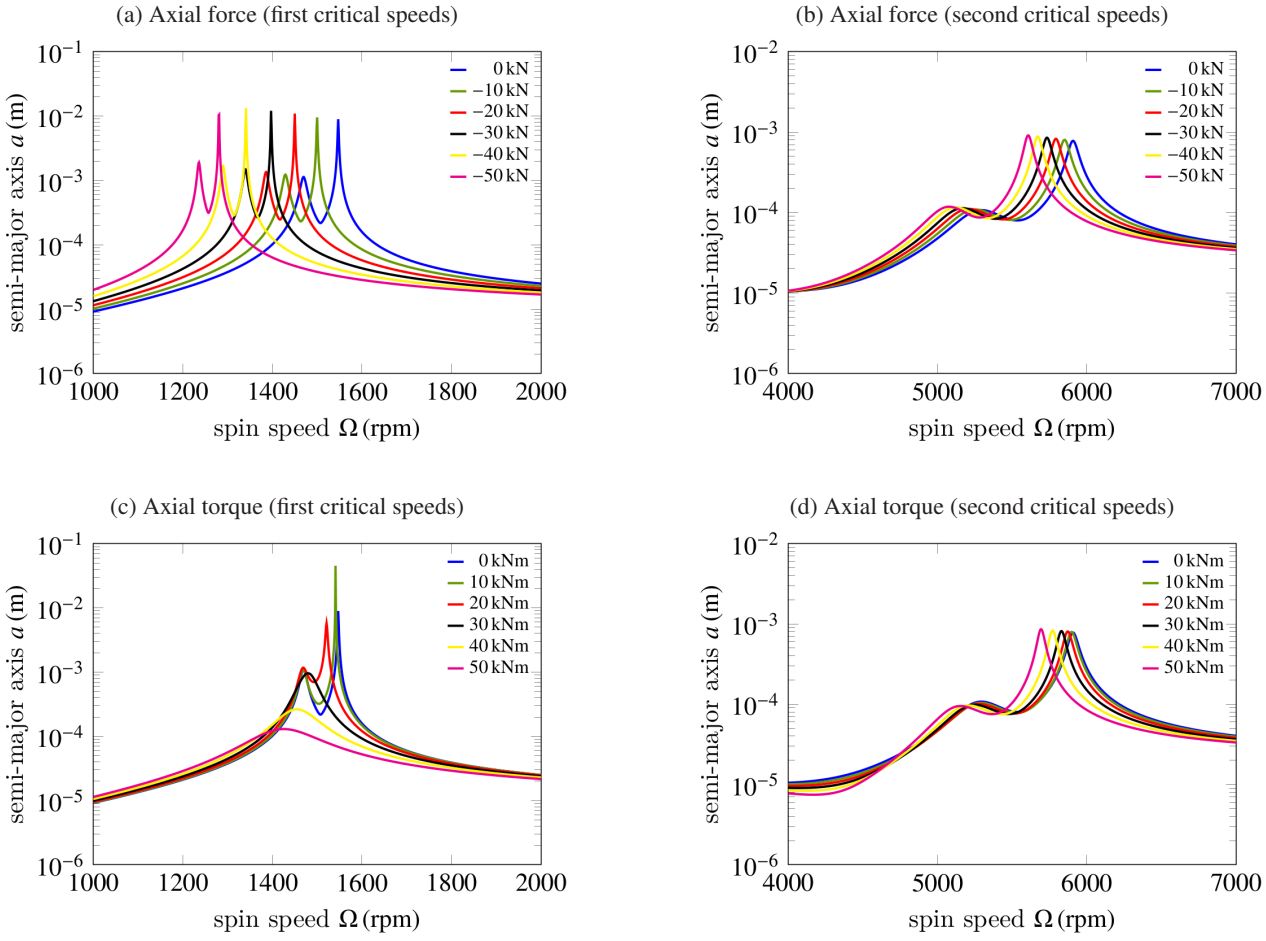

Fig. 3. Effect of axial loading on the unbalance response

Eubanks [21]. Additionally, the axial torque leads to a reduced vibration level for the first critical speeds and for high values of $T > 30$ kNm, the splitting of the first critical speed is not visible (see Fig. 3c).

In Fig. 4, a comparison of NAT and FEM for three different load cases is shown. It is apparent that the results for the semi-major axis (a) and semi-minor axis (b) of the elliptical orbit at $z = 0.46$ m are in excellent agreement for all load cases (no axial loads, $P = -50$ kN, $T = 50$ kNm). An *Intel*® Core™ i7 system (6×3.7 GHz, 32 GB RAM) with a Windows 10 operating system is used to carry out the computations. The computational time of NAT is approximately three times shorter compared to FEM, which shows the computational efficiency of NAT.

In the second numerical example, a more realistic rotor-bearing system is chosen to show the efficiency and accuracy of NAT. The example is similar to the previous one, but has nine rotor segments with different cross-sections and is supported by anisotropic bearings. The system is illustrated in Fig. 5. The parameters of the discs at station (3), (5) and (7) are the same as in Table 1. Each disc has a mass unbalance, which is given by $\varepsilon^{(3)} = 0.03$ mm, $\varepsilon^{(5)} = 0.025$ mm and $\varepsilon^{(7)} = 0.04$ mm and the angular position $\beta^{(3)} = 30°$, $\beta^{(5)} = 90°$ and $\beta^{(7)} = 120°$. A distributed unbalance is omitted in this example. The diameters of the cross-sections are $d_1 = 0.03$ m, $d_2 = 0.04$ m, $d_3 = 0.05$ m, $d_4 = 0.06$ m, $d_5 = 0.07$ m, $d_6 = 0.08$ m, $d_7 = 0.06$ m, $d_8 = 0.04$ m and $d_9 = 0.03$ m. The bearings at the stations (2) and (10) are equal and two different types are examined. To get realistic bearing parameters, the hydrodynamic short width bearing theory presented in [19] is applied. Although, the theory shown in [19] leads to spin speed dependent bearing parameters, constant values are assumed in this paper. The parameter sets listed in Table 2 are calculated with a bearing eccentricity of 0.793 and 0.692 and an assumed constant spin speed of 3000 rpm and 7000 rpm. Due to the minor effects of axial loadings on the rotor-bearing system, as shown in the previous example, the constant axial force and torque are set to zero.

Table 2
Parameters of the anisotropic bearings

Type	k_x	k_y	k_{xy}	k_{yx}	d_x	d_y	$d_{xy} = d_{yx}$
	(kN/m)				(Ns/m)		
1	11600	54400	−3970	−32800	2416	16810	−4005
2	12400	34300	−860	−28000	1487	6292	−1817

In Figs. 6 and 7, the semi-major and semi-minor axis of the elliptical orbits for the first two critical speeds at $z = 0.46$ m are shown. The FEM model used to compute the reference solutions has an element size of 0.01 m (104 elements). The results of NAT and FEM match perfectly for the first critical speed (Figs. 6a and 6b). At the second critical speed some deviations between NAT and FEM are noticeable, which is apparent from Figs. 7a and 7b. Due to the higher spin speed at the second crit-

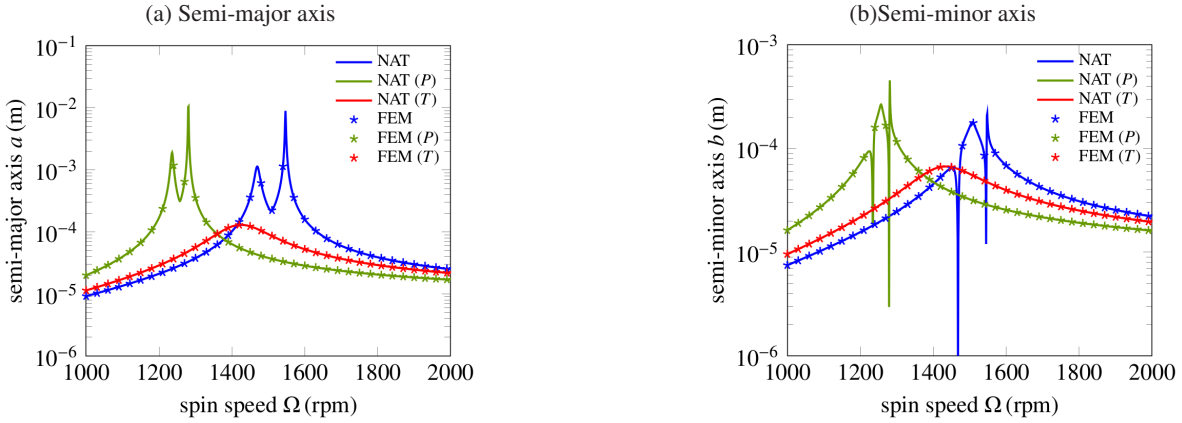

Fig. 4. Comparison of NAT and FEM for different load cases

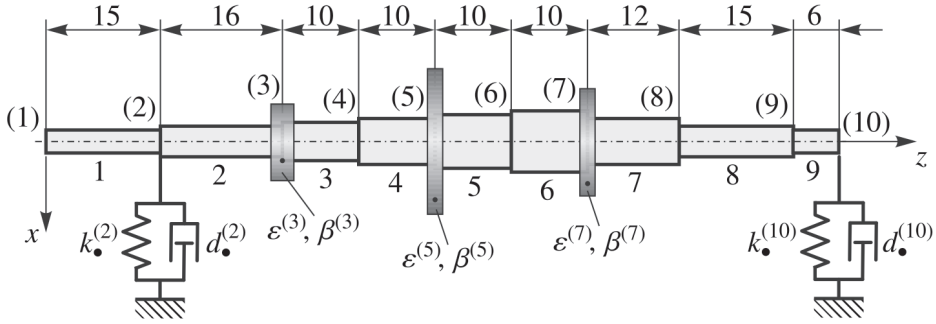

Fig. 5. Configuration of the second example rotor with anisotropic bearings and nine sections

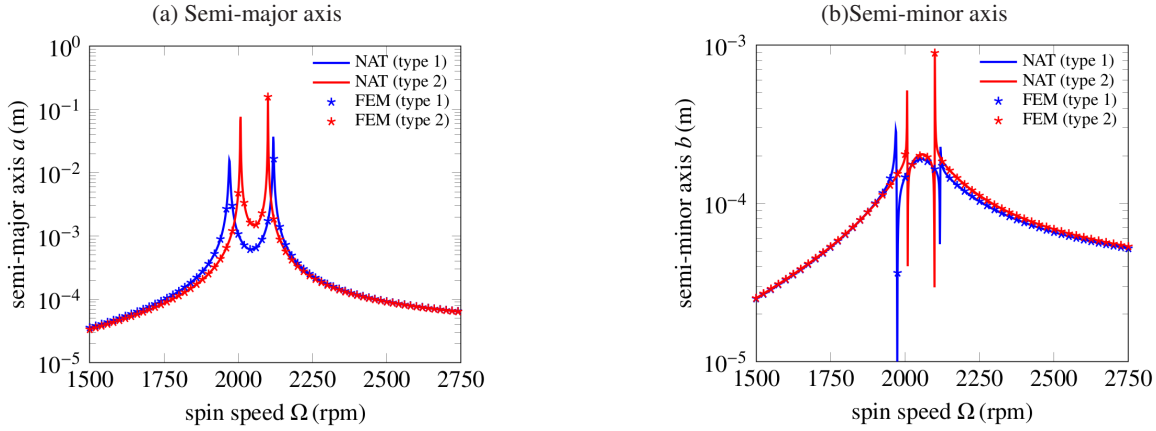

Fig. 6. Comparison of NAT and FEM for the two bearing types (first critical speed)

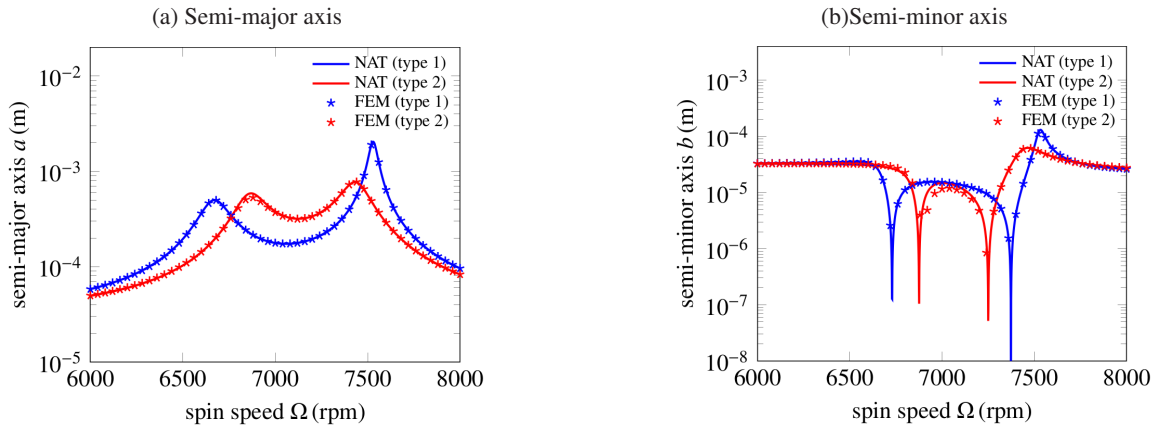

Fig. 7. Comparison of NAT and FEM for the two bearing types (second critical speed)

ical speed, the element size of the FEM reference model is not small enough to accurately represent the deformation. It can be shown that the FEM solution converges towards the results of NAT with decreasing element size. Even though, the number of segments in the second example is much higher compared to the first one, the computation time of NAT is still approximately 2.5 times lower compared to FEM. NAT requires 31 s to calculate 10 000 points of the unbalance response curve, while the computation time of FEM is 78 s. This clearly shows the efficiency of NAT compared to FEM. Furthermore, the solutions of NAT are quasi-analytical, since errors are only introduced in the approximation of the unbalance distribution, while the governing equations are fulfilled exactly. This has considerable advantages for the calculation of derived quantities, e.g. bending moments or shear forces, since high accuracy is achieved, while FEM loses accuracy due to a lower order approximation of these quantities.

5. CONCLUSION

In this paper, an extension of NAT to rotating Rayleigh beams under constant axial loading running in general anisotropic bearings with cross-coupling effects has been developed. The numerical examples have shown that the numerical efficiency and accuracy of NAT is not influenced by the additional effects. The calculated unbalance response illustrates the effects of a constant axial compression force and axial torque on the critical speeds of a rotor-bearing system. The critical speeds are lower by both loadings, which is in agreement with previous results in the literature.

ACKNOWLEDGEMENTS

The authors acknowledge the financial support by Graz University of Technology Open Access Publishing Fund.

REFERENCES

[1] J.W. Lund and F.K. Orcutt, "Calculations and Experiments on the Unbalance Response of a Flexible Rotor," *J. Eng. Ind.*, vol. 89, no. 4, pp. 785–796, 1967.

[2] A. Vollan and L. Komzsik, *Computational Techniques of Rotor Dynamics with the Finite Element Method*. Boca Raton: CRC Press, 2012.

[3] J.S. Rao, *Rotor Dynamics*. New Delhi: New Age International, 1996.

[4] A.-C. Lee and Y.-P. Shih, "The Analysis of Linear Rotor-Bearing Systems: A General Transfer Matrix Method," *J. Vib. Acoust.*, vol. 115, no. 4, pp. 490–497, 1993.

[5] T. Yang and C. Lin, "Estimation of Distributed Unbalance of Rotors," *J. Eng. Gas Turbines Power*, vol. 124, no. 4, pp. 976–983, 2002.

[6] J.-S. Wu and H.-M. Chou, "A new approach for determining the natural frequencies and mode shapes of a uniform beam carrying any number of sprung masses," *J. Sound Vib.*, vol. 81, no. 3, pp. 1–10, 1999.

[7] J.-S. Wu, F.-T. Lin, and H.-J. Shaw, "Analytical Solution for Whirling Speeds and Mode Shapes of a Distributed-Mass Shaft With Arbitrary Rigid Disks," *J. Appl. Mech.*, vol. 220, no. 3, pp. 451–468, 2014.

[8] M. Klanner and K. Ellermann, "Steady-state linear harmonic vibrations of multiple-stepped Euler-Bernoulli beams under arbitrarily distributed loads carrying any number of concentrated elements," *Appl. Comput. Mech.*, vol. 14, no. 1, pp. 31–50, 2020.

[9] M. Klanner, M.S. Prem, and K. Ellermann, "Steady-state harmonic vibrations of a linear rotor-bearing system with a discontinuous shaft and arbitrary distributed mass unbalance," in *Proceedings of ISMA2020 International Conference on Noise and Vibration Engineering and USD2020 International Conference on Uncertainty in Structural Dynamics*, Leuven, Belgium, Sep. 2020, pp. 1257–1272.

[10] H. Ziegler, "Knickung gerader Stäbe unter Torsion," *J. Appl. Math. Phys. (ZAMP)*, vol. 3, pp. 96–119, 1952.

[11] V.V. Bolotin, *Nonconservative Problems of the Theory of Elastic Stability*. New York: Pergamon Press, 1963.

[12] H. Ziegler, *Principles of Structural Stability*. Basel: Springer Basel AG, 1977.

[13] L. Debnath and D. Bhatta, *Integral Transforms and Their Applications*. CRC Press, 2015.

[14] D. Mitrinović and J.D. Kečkić, *The Cauchy Method of Residues*. D. Reidel Publishing, 1984.

[15] S.I. Hayek, *Advanced Mathematical Methods in Science and Engineering*. CRC Press, 2010.

[16] B. Adcock, D. Huybrechs, and J. Martín-Vaquero, "On the Numerical Stability of Fourier Extensions," *Found. Comput. Math.*, vol. 14, no. 4, pp. 638–687, 2014.

[17] R. Matthysen and D. Huybrechs, "Fast Algorithms for the Computation of Fourier Extensions of Arbitrary Length," *SIAM J. Sci. Comput.*, vol. 38, no. 2, pp. A899–A922, 2016.

[18] A.-C. Lee, Y. Kang, and L. Shin-Li, "A Modified Transfer Matrix Method for Linear Rotor-Bearing Systems," *J. Appl. Mech.*, vol. 58, no. 3, pp. 776–783, 1991.

[19] M.I. Friswell, J.E. T. Penny, S.D. Garvey, and A.W. Lees, *Dynamics of Rotating Machines*. New York: Cambridge University Press, 2010.

[20] A. De Felice and S. Sorrentino, "On the dynamic behaviour of rotating shaftsunder combined axial and torsional loads," *Meccanica*, vol. 54, no. 7, pp. 1029–1055, 2019.

[21] R.L. Eshleman and R.A. Eubanks, "On the Critical Speeds of a Continuous Rotor," *J. Manuf. Sci. Eng.*, vol. 91, no. 4, pp. 1180–1188, 1969.